Exchange bias effect in partially oxidized amorphous Fe–Ni–B based metallic glass nanostructures

2012 J. Phys.: Condens. Matter 24 256004

(http://iopscience.iop.org/0953-8984/24/25/256004)

J. Phys.: Condens. Matter **24** (2012) 256004 (8pp) doi:10.1088/0953-8984/24/25/256004

Exchange bias effect in partially oxidized amorphous Fe–Ni–B based metallic glass nanostructures

S Thomas[1], G Pookat[2], S S Nair[3], M Daniel[1], B Dymerska[4], A Liebig[1], S H Al-Harthi[5], R V Ramanujan[6], M R Anantharaman[2], J Fidler[4] and M Albrecht[1]

[1] Institute of Physics, Chemnitz University of Technology, 09107 Chemnitz, Germany
[2] Department of Physics, Cochin University of Science and Technology, 682022 Cochin, India
[3] I3N and CICECO, Universidade de Aveiro, 3810-193 Aveiro, Portugal
[4] Institute of Solid State Physics, Vienna University of Technology, Wiener Hauptstrasse 8-10, 1040 Vienna, Austria
[5] Department of Physics, Sultan Qaboos University, 123 Muscat, Sultanate of Oman
[6] School of Materials Science and Engineering, Nanyang Technological University, 639798 Singapore, Singapore

E-mail: senoy.thomas@physik.tu-chemnitz.de

Received 27 February 2012, in final form 4 May 2012
Published 25 May 2012
Online at stacks.iop.org/JPhysCM/24/256004

Abstract
The magnetic properties of amorphous Fe–Ni–B based metallic glass nanostructures were investigated. The nanostructures underwent a spin-glass transition at temperatures below 100 K and revealed an irreversible temperature following the linear de Almeida–Thouless dependence. When the nanostructures were cooled below 25 K in a magnetic field, they exhibited an exchange bias effect with enhanced coercivity. The observed onset of exchange bias is associated with the coexistence of the spin-glass phase along with the appearance of another spin-glass phase formed by oxidation of the structurally disordered surface layer, displaying a distinct training effect and cooling field dependence. The latter showed a maximum in exchange bias field and coercivity, which is probably due to competing multiple equivalent spin configurations at the boundary between the two spin-glass phases.

(Some figures may appear in colour only in the online journal)

1. Introduction

Exchange coupling between a ferromagnet (FM) and an antiferromagnetic layer can give rise to a unidirectional anisotropy referred to as exchange bias [1–4], which is manifested as an enhancement in coercive force and, more significantly, as a shift of the hysteresis loop along the field axis. Co–CoO core–shell particles were the first type of system where the exchange bias effect was reported [5]. Since then, extensive research activities have been carried out to understand the underlying phenomena [2]. The driving force for improving the performance of permanent magnets [6] and the need to combat the superparamagnetic limit [7] in magnetic recording media propelled further research in this direction. Consequently, exchange bias effects were observed in many other types of nanoparticle system such as surface modified nanoparticles [8–11], ferromagnetic nanoparticles embedded in an antiferromagnetic matrix [12] and core–shell nanoparticles [13, 14], as well as in ferrimagnetic–antiferromagnetic heterostructures [15].

Recently, exchange bias effects have also been reported in ferromagnets in contact with a spin-glass (SG) [16]. When an FM–SG system is cooled in a magnetic field across the SG transition temperature, some of the spins of the SG phase will be aligned and frozen in the direction of the cooling field. During magnetization reversal in an applied field, some of the spins of the SG phase keep their direction and pin the FM spins, which results in a shift of the measured hysteresis

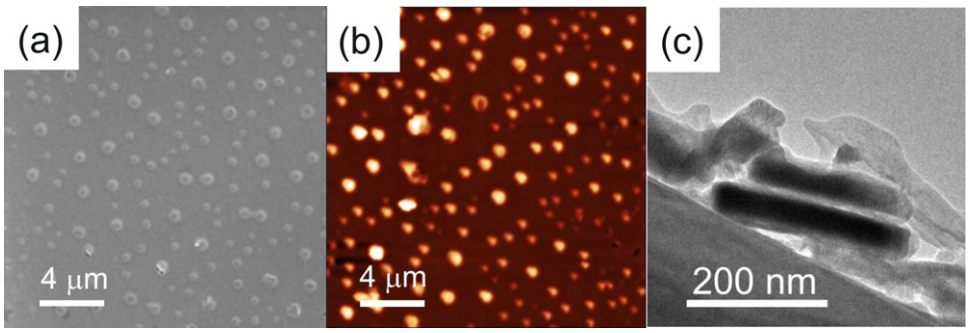

Figure 1. (a) SEM image, (b) AFM image, and (c) TEM cross-sectional image of Fe–Ni–B based nanostructures.

loop. Depending on the cooling field and on the temperature at which the field is applied, the degeneracy of the SG can be reduced, and even destroyed at higher fields. Hence in FM–SG systems the magneto-thermal history of the sample has a strong influence on the exchange bias properties. In this regard, a cooling field dependent exchange bias was observed in Fe–Fe oxide systems, where the magnitude of the exchange bias field showed a maximum [17]. Furthermore, in γ-Fe_2O_3 coated Fe nanoparticles a strong training effect was reported [18]. Field cooled hysteresis loop shifts in both horizontal and vertical directions were associated with the frozen spins, whose configuration was changing with the field cycling during hysteresis loop measurements.

In this paper, we report on the exchange bias effect in amorphous Fe–Ni–B based metallic glass nanostructures, which are in an SG state at temperatures below 100 K. The oxidized and structurally disordered surface layer of the nanostructures revealed an onset of spin freezing below 25 K, and via exchange coupling of the two different SG phases exchange biased heterostructures are formed.

2. Experimental details

Commercially available Metglas 2826 MB ribbon of composition $Fe_{40}Ni_{38}Mo_4B_{18}$ was employed as a source material to deposit Fe–Ni–B based amorphous thin films. The films were deposited at room temperature on naturally oxidized Si(100) substrates by thermal evaporation at a pressure of about 2×10^{-5} mbar. Synchrotron x-ray diffraction measurements in gracing incidence geometry performed at beamline G3 of HASYLAB at DESY (Hamburg, Germany) confirmed the amorphous nature of the samples (not shown). The chemical composition of the surface was studied by x-ray photoelectron spectroscopy (XPS) with a monochromatic Al Kα x-ray source of energy 1486.6 eV. Atomic force microscopy (AFM) studies were carried out using a Digital Instruments multimode scanning probe microscope operated under ambient conditions. Scanning electron microscopy (SEM) was performed with a Philips NanoNova system. The analysis of the microstructure was carried out by transmission electron microscopy (TEM, FEI F20) operated at 200 kV. The TEM specimens were prepared conventionally followed by a standard ion polishing procedure. Ferromagnetic resonance (FMR) measurements were made on a Bruker ESP 300E spectrometer, operating in the X-band (9.47 GHz) at room temperature. Temperature dependent magnetic properties were measured using a superconducting quantum interference device vibrating sample magnetometer (SQUID VSM, Quantum Design).

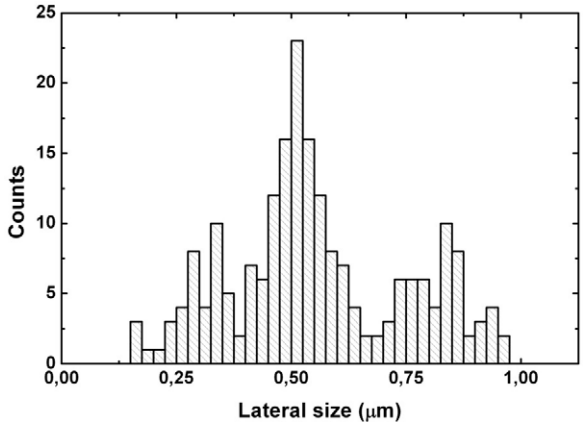

Figure 2. Lateral size distribution of Fe–Ni–B based nanostructures extracted from SEM images.

3. Results and discussion

3.1. Structure and composition

After the film deposition at room temperature, the surface was analyzed by AFM and SEM. Interestingly, as depicted in the SEM image of figure 1(a), nanostructures are formed on the substrate surface. Reasons for the nanostructure formation are not yet clear, but it is expected that sample heating via the evaporation source is most likely. The area fraction of the nanostructures on the substrate surface is about 11%, showing large separations between them. Figure 1(b) shows an AFM image acquired from the same sample. Combination of the two imaging techniques provides information on the lateral size, height and area coverage of the nanostructures. A statistical analysis of the SEM images revealed a broad distribution in lateral size of the nanostructures with sizes between 200 nm and 1 μm (see figure 2). It was also observed from AFM images that there is a distribution in their height, varying from 25 nm up to 100 nm with

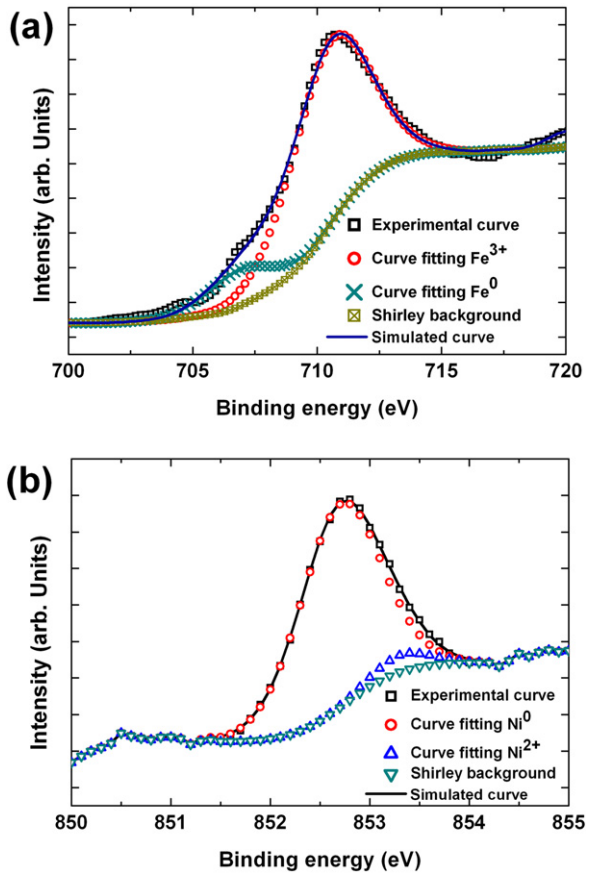

Figure 3. XPS spectra of Fe–Ni–B based nanostructures recorded around (a) the Fe 2p and (b) Ni 2p lines. The fitting of the spectra clearly confirms the presence of Fe^0/Fe^{3+} and indicates the presence of Ni^{2+} together with Ni^0.

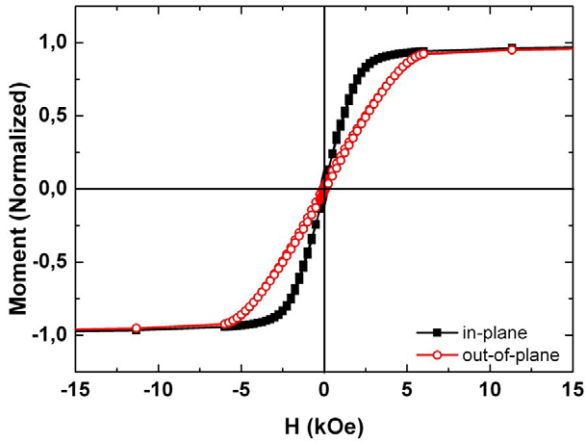

Figure 4. *M–H* loops (normalized to the saturation moment) for Fe–Ni–B based nanostructures recorded in in-plane and out-of-plane geometry at room temperature.

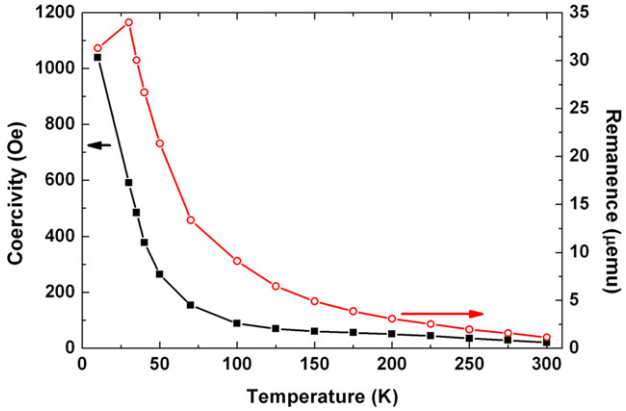

Figure 5. Temperature dependence of coercivity (filled square) and remanence (open circle) after zero-field cooling.

increasing lateral size. This can also be seen in the TEM image presented in figure 1(c), showing a cross-sectional view of two nanostructures, which were detached from the substrate surface during TEM specimen preparation.

The chemical composition of the nanostructures in particular at the surface was analyzed by XPS. Figures 3(a) and (b) show high-resolution XPS spectra recorded at the characteristic Fe 2p and Ni 2p lines. Curve fitting to the XPS spectra revealed clearly that the Fe $2p_{3/2}$ and Ni $2p_{3/2}$ peak can be deconvoluted to Fe^0/Fe^{3+} and Ni^0/Ni^{2+} components, respectively, confirming the formation of a native oxide layer on the surface. The presence of a small percentage of NiO cannot be ruled out, as the Ni 2p line showed a small component of Ni^{2+}. The presence of Fe^{3+} and Ni^{2+} indicates the formation of structurally disordered mixed oxides (mostly Fe_2O_3 along with a small percentage of NiO). This surface oxide layer is now exchange coupled to the Fe–Ni–B layer and might become magnetically ordered at low temperatures, which in turn can give rise to an exchange bias effect [10].

3.2. Magnetic properties

Figure 4 shows *M–H* hysteresis loops of the prepared Fe–Ni–B sample recorded at room temperature for an external magnetic field applied parallel (in-plane) and perpendicular (out-of-plane) to the substrate plane. The loops nearly saturate above 5 kOe and possess low coercivity and remanence in both directions due to the randomness in magnetization orientation. The difference in susceptibility along the two directions is simply given by the shape anisotropy. This behavior was further confirmed by angular dependent FMR measurements in out-of-plane geometry. The out-of-plane angular dependence of the resonance field suggested a random orientation of spins in these structures (results are not shown). The temperature dependence of the magnetic properties in the in-plane field direction was determined by *M–H* loop measurements after zero-field cooling, revealing an enhancement in coercivity as well as in remanence, in particular below 100 K, with decreasing temperature, as summarized in figure 5.

In order to get a better understanding of the mechanism which is responsible for this behavior, field cooling (FC) and zero-field cooling (ZFC) magnetization measurements were performed under different applied fields. For ZFC measurements, first the sample was cooled from 300 to 10 K in zero magnetic field and then at 10 K a magnetic field was applied. The magnetic moment was recorded on warming the

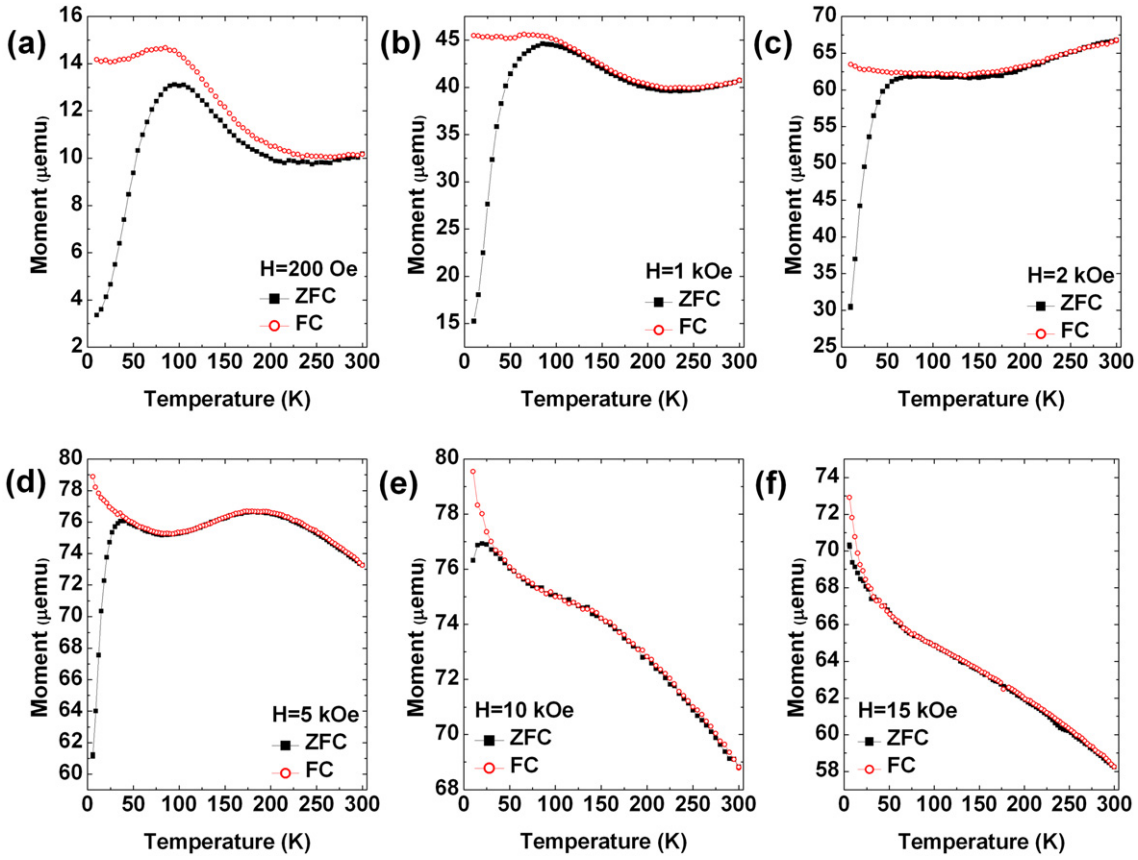

Figure 6. FC and ZFC curves measured at (a) 200 Oe, (b) 1 kOe, (c) 2 kOe, (d) 5 kOe, (e) 10 kOe, and (f) 15 kOe.

sample to 300 K (ZFC curve, M_{ZFC}). The magnetic moment was measured again by cooling the sample to 10 K, keeping the applied field unchanged (FC curve, M_{FC}). Figure 6 shows the temperature dependence of FC and ZFC magnetizations for different fields ranging from 200 Oe to 15 kOe, revealing a bifurcation between FC and ZFC data at an irreversibility temperature T_{irr}. It has to be noted that the difference between the values of M_{FC} and M_{ZFC} at a given temperature is a direct measure of the irreversibility in magnetization at that temperature. In this regard, a SG phase is characterized by the field dependence of T_{irr} [19]. For Ising spin systems, de Almeida and Thouless have predicted a $\frac{H}{\Delta J} \propto (1 - \frac{T_{\mathrm{irr}}}{T_{\mathrm{F}}})^{3/2}$ dependence of T_{irr} on H, where T_{F} is the zero-field SG freezing temperature and ΔJ the width of the distribution of exchange interactions [20].

Figure 7 shows $H^{2/3}$ as a function of T_{irr}. This plot exhibits a linear dependence in agreement with the predictions of de Almeida and Thouless. The linear fit to the experimental data is extrapolated to $H = 0$ to obtain the zero-field SG transition (T_{F}), giving a value of T_{F} equal to 102 K. Furthermore, extrapolation of the linear fit back to $T = 0$ allows us to estimate the critical field above which the SG phase vanishes, which appears at about 12 kOe. These results show that at temperatures below ∼100 K, when applying small magnetic fields, the system is in an SG state and it costs more field strength to rotate the frozen spins in the magnetic field direction, which results in a coercivity enhancement at temperatures below 100 K [21]. Even though this SG

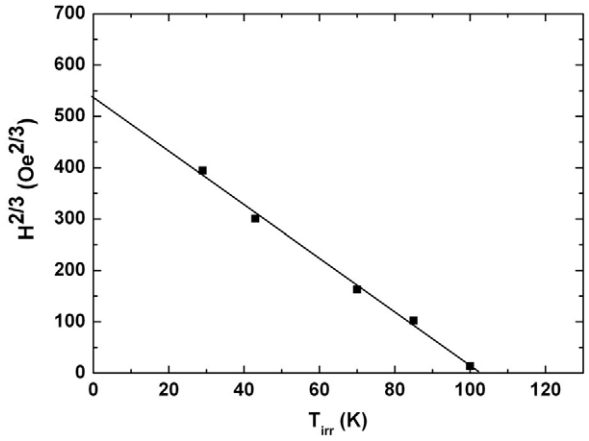

Figure 7. $H^{2/3}$ versus T_{irr} plot following the linear de Almeida–Thouless dependence.

phase is expected to disappear at magnetic fields larger than 12 kOe, FC–ZFC magnetization measurements obtained at $H = 15$ kOe (see figure 6(f)) reveal an irreversibility in magnetization at temperatures below 25 K. This behavior will be discussed in detail later.

The existence of an SG phase can be further evidenced from the high-field relaxation process in alternating fields after zero-field cooling. For this, the sample was first cooled to 10 K in zero field; at 10 K, a magnetic field of 10 kOe was applied and then the magnetic moment was measured

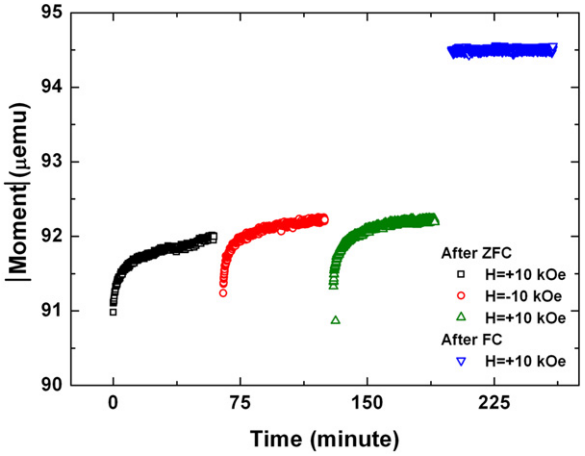

Figure 8. Time dependence of the magnetic moment measured at 10 K in various applied magnetic fields after zero-field cooling. It has to be noted that absolute values are presented in order to allow for a comparison between 10 and −10 kOe curves. Furthermore, the time dependence of magnetization in a field of 10 kOe after field cooling (at 10 kOe) is also shown.

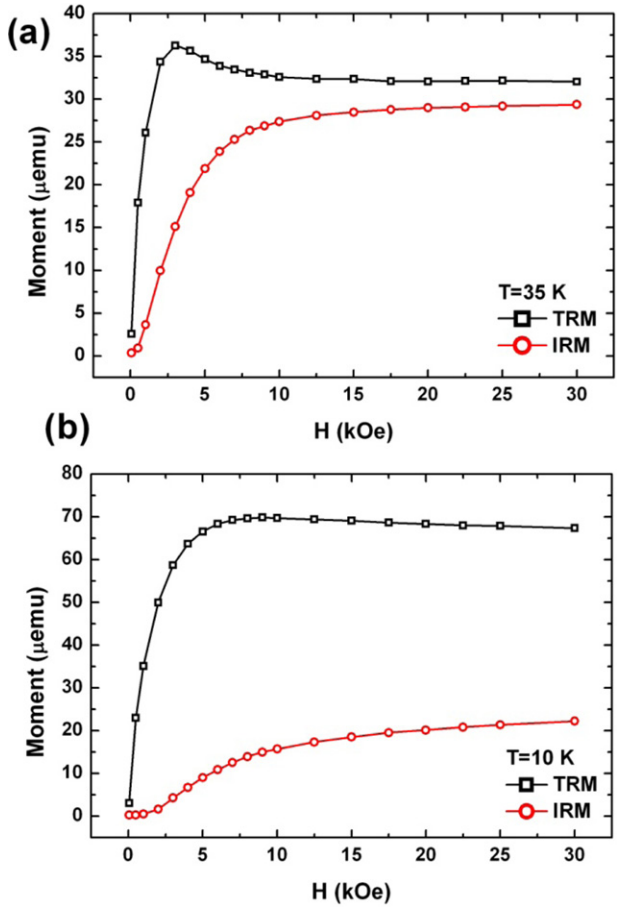

Figure 9. TRM and IRM curves measured at (a) 35 K and (b) 10 K.

as a function of time (up to 60 min). After this, the field direction was reversed (−10 kOe), followed by the recording of the magnetic moment as a function of time. Finally, the magnetic field was again reversed to 10 kOe while continuing the recording of the magnetic moment as a function of time. The result of this measurement is summarized in figure 8.

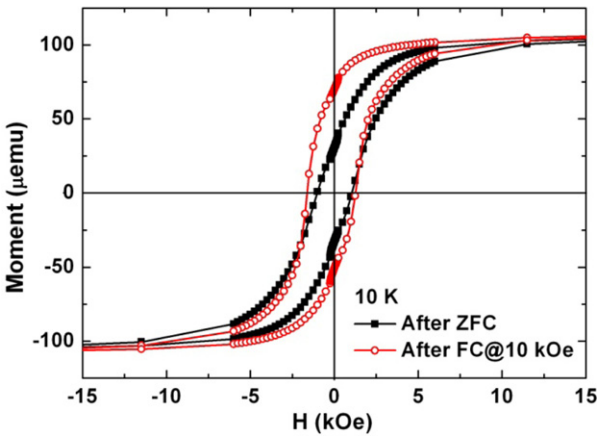

Figure 10. *M–H* loops for Fe–Ni–B based nanostructures recorded in in-plane geometry at 10 K after ZFC and FC procedures.

An upward rise in magnetization with time after the ZFC procedure indicates a gradual orientation of spins towards the field direction. For comparison, the magnetic moment at 10 kOe was also measured at 10 K after field cooling in a field of 10 kOe. In this case, the moment is independent of time, which means that the field cooling process has already established an equilibrium magnetization state.

In this regard, it is well known that the magnetic behavior of an SG depends on whether it is cooled in a field or not [22]. This behavior is also expressed in differences in thermo-remanent magnetization (TRM) and isothermal remanent magnetization (IRM) curves. TRM and IRM curves were measured as functions of field and temperature. For the TRM measurement, the system was cooled (35 K min^{-1}) in an external magnetic field; when the measurement temperature was reached, the field was switched off and the magnetic moment was measured, giving the TRM at this particular initial field value. For the IRM measurement, the system was cooled (35 K min^{-1}) in zero external field, and when the measuring temperature was reached a magnetic field was applied for a short interval of 10 s. Again, the magnetic moment is measured once the field is switched off, giving the IRM. Figure 9(a) shows TRM/IRM curves obtained at 35 K as a function of magnetic field.

As can be seen, the TRM curve grows steeply with field and exhibits a characteristic peak at ∼3 kOe. At this point the magnetic field energy is of the order of the interaction energy ($\sim k_B T_F$) [22]. The interaction field is assumed to be negative and increases as the field increases, which in turn decreases TRM at higher cooling fields [23]. In contrast, the IRM curve increases with field and approaches the value of TRM at higher fields. Please note that larger TRM values are expected in comparison to IRM values, as TRM starts from a higher magnetization state. Figure 9(b) shows TRM/IRM curves measured at 10 K. In this case, the TRM and IRM curves are not coinciding even at high fields. This behavior indicates the presence of an additional anisotropy contribution appearing already at low temperatures.

In order to understand this behavior, *M–H* loops were recorded at 10 K after field cooling (10 kOe) from 300 K. The result is shown in figure 10 along with a hysteresis

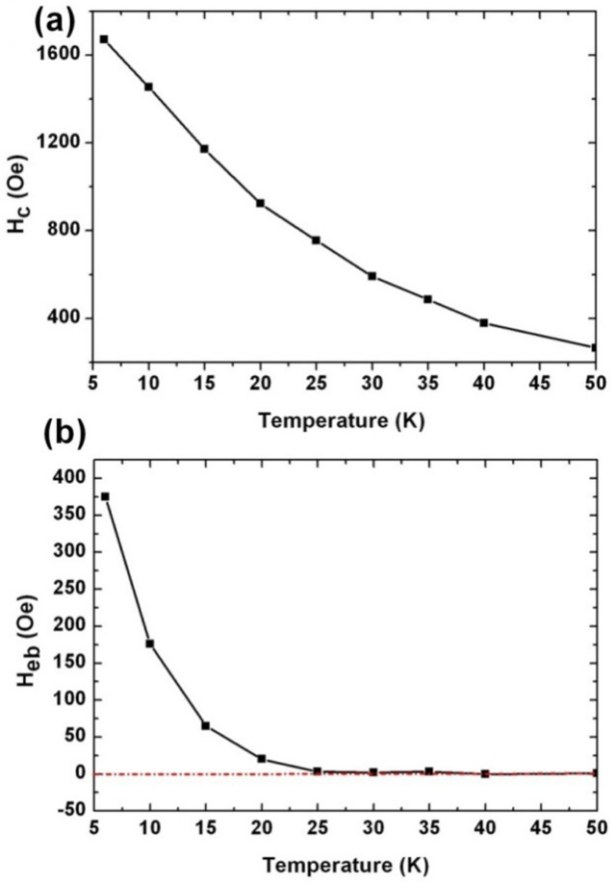

Figure 11. (a) H_c and (b) H_{eb} plotted as a function of temperature. The sample was field cooled from 300 K in 10 kOe.

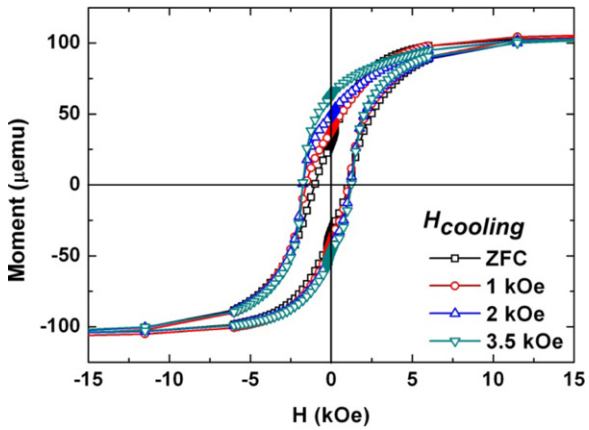

Figure 12. *M–H* loops for Fe–Ni–B based nanostructures recorded in in-plane geometry at 10 K taken after cooling in different cooling fields.

loop recorded after ZFC. A clear shift in the hysteresis loop opposite to the cooling field direction by 170 Oe and an increase in coercivity after field cooling are observed, which confirms the presence of exchange bias. This effect might be induced by the onset of spin freezing of the SG surface layer. From figure 6(f) it has already been observed that there is an irreversible magnetization contribution visible at 15 kOe for temperatures less than 25 K. This means that, even after the disappearance of the SG phase at about 12 kOe, some frozen high anisotropy spins do exist, which contribute to the irreversible magnetization. The irreversibility in FC and ZFC magnetization was present even at 50 kOe. Previously, in ferrite nanoparticles, such a high-field irreversibility in FC and ZFC magnetization was attributed to an SG-like behavior of the surface layer [24–26].

Figure 11(a) shows the temperature evolution of the coercivity H_c defined as $H_c = \frac{H_{c2}-H_{c1}}{2}$, and figure 11(b) presents the temperature dependence of the exchange bias field H_{eb}, $[H_{eb} = -(\frac{H_{c1}+H_{c2}}{2})]$, where H_{c1} is the coercivity of the descending branch and H_{c2} is the coercivity of the ascending branch of the *M–H* loop. A clear onset of exchange bias at around 25 K was observed.

Furthermore, a drastic increase in remanence is obtained after FC (see figure 10). At room temperature the applied cooling field will align the spins of the nanostructures, and with reducing temperature the spins will be progressively frozen in a disordered state, seeking the lowest energy configuration. Apparently, more spins are aligned in the field direction after field cooling, lifting the initial randomness of the exchange anisotropy. Thus, it is expected that the magnitude of cooling field will have a strong influence on the exchange bias.

Figure 12 shows *M–H* loops recorded at 10 K for different cooling fields, $H_{cooling}$, ranging from 0 to 3.5 kOe. For ZFC samples, the *M–H* loop is symmetric. This is expected for a sample with randomly oriented moments. In this case the unidirectional anisotropy, resulting from the exchange bias effect, will be cancelled out, leading to a symmetrical hysteresis loop. For higher cooling fields one can see that the loops are becoming more asymmetric. In figure 13 the remanence of the descending branch, coercive fields (H_{c1}, H_{c2}, and H_c) and the exchange bias field, H_{eb}, are plotted as a function of $H_{cooling}$. The following findings can be extracted from the figures: (i) the magnitude of H_{c1} steeply increases with cooling field up to 2 kOe and then gradually decreases from 3.5 kOe onwards, (ii) the magnitude of H_{c2} steeply increases with cooling field up to 5 kOe and then it remains unchanged, (iii) H_{eb} and H_c curves show a peak at $H_{cooling} \sim 3$ kOe, and (iv) the remanence of the magnetization curve increases for cooling fields up to 10 kOe and then gradually decreases.

As already mentioned, more spins will be aligned in the field direction after field cooling, lifting the initial randomness of the exchange anisotropy. Therefore, an initial increase in remanence is expected, which is accompanied by an increase in exchange bias and coercivity. However, at larger cooling fields also spins that are pinned due to magnetic interactions inside the SG–SG system, which can be very manifold, will be partially aligned, and during freezing a spin configuration which is not in a minimum energy state is generated. Such an effect will certainly reduce the exchange bias field and coercivity. Furthermore, at zero field due to the internal magnetic interactions some spin reorientation will take place, lowering the remanence. To sum up, there is a critical cooling field above which the internal magnetic interactions in the SG–SG systems can be overcome by the Zeeman interaction,

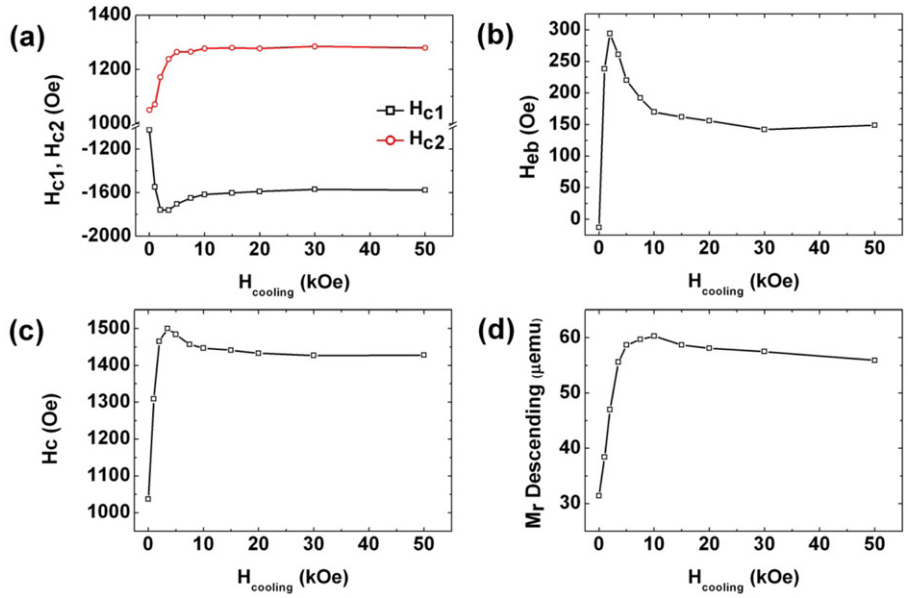

Figure 13. Cooling field, H_{cooling}, dependence of (a) H_{c1}, H_{c2}, (b) H_{eb}, (c) H_{c}, and (d) remanence measured at 10 K.

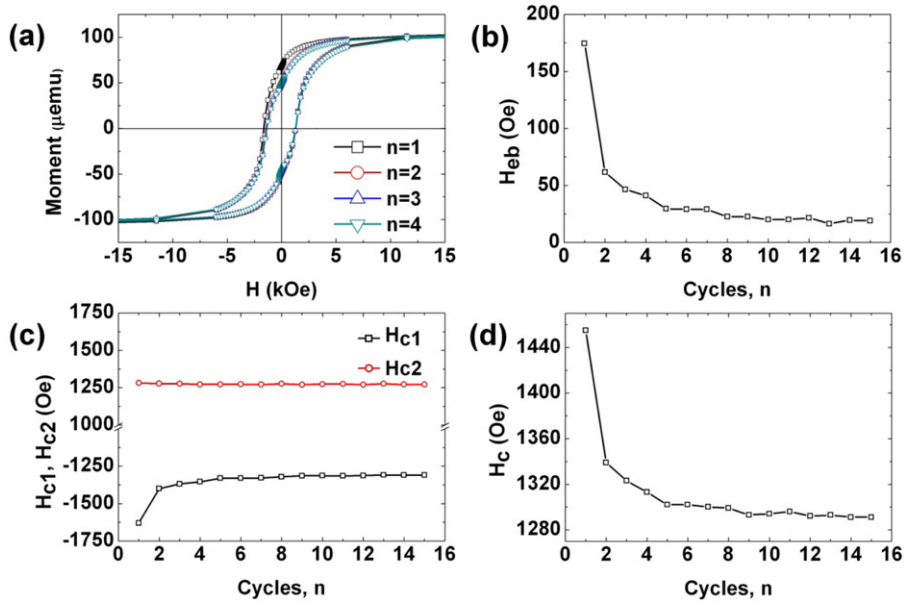

Figure 14. (a) M–H loops recorded for different loop cycles, (b)–(d) dependence of H_{eb} (b), H_{c1}, H_{c2} (c) and H_{c} (d) on loop cycles.

leading to enhanced spin frustration in the frozen magnetic spin configuration, thus reducing the exchange bias. Below this critical field, the Zeeman interaction is not strong enough to overcome the internal magnetic interactions and lowers only the randomness of the exchange anisotropy, which results in an increase in exchange bias. Very similar results have been observed in a granular system of Fe nanoparticles embedded in an SG-like Fe oxide matrix [17].

From our discussion it is clear that the spin configuration of the SG–SG heterostructure deviates from its equilibrium configuration. Therefore, we trained the system by increasing the number of loop cycles while measuring the exchange bias and coercivity. A variation of these quantities as a function of loop cycles is a direct macroscopic fingerprint of configurational rearrangements of the spin structure towards equilibrium. Figure 14(a) shows M–H loops measured after different loop cycles, n (=1–4), revealing a clear training effect, which can be better seen in the variation of H_{eb} and H_{c} (see figures 14(b), (d)), where both parameters decrease with increasing loop cycles. Please note that the training effect is more pronounced in the descending branch of the M–H loop (figure 14(c)). The magnitude of H_{c1} decreases significantly in the first field cycle itself, while H_{c2} remains unchanged with increasing n. Figure 15 shows the normalized residual training $[(H^n_{\text{eb}} - H^{15}_{\text{eb}})/(H^1_{\text{eb}} - H^{15}_{\text{eb}})]$ as a function of $\frac{1}{\sqrt{n}}$. Here, H^n_{eb} is the exchange bias field for the nth loop cycle. The solid line in figure 15 is a linear fit to the experimental data following

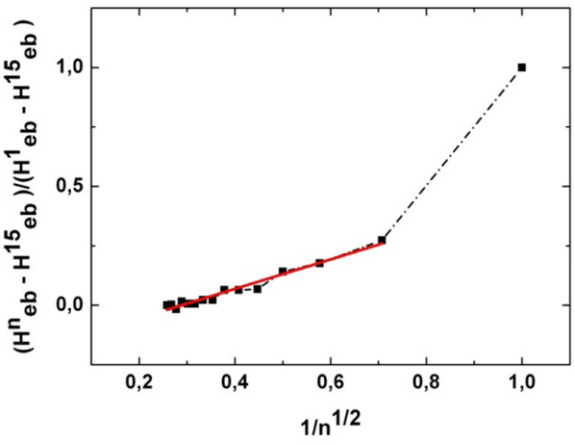

Figure 15. Residual training normalized to the total extent of training $[(H^n_{eb} - H^{15}_{eb})/(H^1_{eb} - H^{15}_{eb})]$ plotted as a function of $\frac{1}{\sqrt{n}}$.

a power law $H^n_{eb} - H^{15}_{eb} \propto \frac{1}{\sqrt{n}}$ (for $n = 2$–15) as introduced by Binek [27]. As an SG is characterized by the presence of multiple configurations of its ground state [19], some of the frozen spins, which were aligned in the cooling field direction, may change their direction and fall into other metastable configurations during field cycling. It is this reconfiguration of frozen spins which results in a decrease of H_{eb} during field cycling. A similar reason was suggested for the training effect of exchange biased γ-Fe_2O_3 coated Fe nanoparticles [18].

4. Conclusions

We investigated the magnetic properties of partially oxidized Fe–Ni–B based magnetic nanostructures. Magnetic measurements after zero-field cooling revealed an increase in coercivity for temperatures less than 100 K, which is ascribed to the SG ordering of the nanostructures. The SG nature is demonstrated by the field dependence of T_F following the well known de Almeida–Thouless dependence. Field cooled *M*–*H* loop measurements at temperatures less than 25 K confirm exchange bias with an enhancement in coercive field as well as a shift in the *M*–*H* loop along the field axis. We associated the observed exchange bias with the exchange coupling between the SG phase and a surface SG phase formed by oxidation of the structurally disordered surface layer. The unique SG–SG heterostructure exhibited a distinct cooling field dependence of H_{eb} and H_c with a characteristic peak at ∼3 kOe, which is attributed to the competition between the Zeeman interaction and internal magnetic interactions. A training effect was observed in the first loop cycle itself, and for subsequent loop cycles the normalized residual training followed a power law.

Acknowledgments

The authors acknowledge B Mainz (TU Chemnitz, Germany) for SEM and EDS measurements. MRA acknowledges the support received through the DST–DAAD exchange program.

References

[1] Nogués J and Schuller I K 1999 *J. Magn. Magn. Mater.* **192** 203
[2] Nogués J, Sort J, Langlais V, Skumryev V, Suriñach S, Muñoz J S and Baró M D 2005 *Phys. Rep.* **422** 65
[3] Stamps R L 2000 *J. Phys. D: Appl. Phys.* **33** R247
[4] Radu F and Zabel H 2008 *Springer Tracts Mod. Phys.* **227** 97
[5] Meiklejohn W H and Bean C P 1956 *Phys. Rev.* **102** 1413
[6] Fullerton E E, Jiang J S and Bader S D 1999 *J. Magn. Magn. Mater.* **200** 392
[7] Skumryev V, Stoyanov S, Zhang Y, Hadjipanayis G, Givord D and Nogués J 2003 *Nature* **423** 850
[8] Wang H, Zhu T, Zhao K, Wang W N, Wang C S, Wang Y J and Zhan W S 2004 *Phys. Rev.* B **70** 092409
[9] Fiorani D, Del Bianco L, Testa A M and Trohidou K N 2006 *Phys. Rev.* B **73** 092403
[10] Vasilakaki M and Trohidou K N 2009 *Phys. Rev.* B **79** 144402
[11] Ong Q K, Wei A and Lin X-M 2009 *Phys. Rev.* B **80** 134418
[12] Sort J, Langlais V, Doppiu S, Dieny B, Suriñach S, Muñoz J S, Baró M D, Laurent C and Nogués J 2004 *Nanotechnology* **15** S211
[13] Panagiotopoulos I, Basina G, Alexandrakis V, Devlin E, Hadjipanayis G, Colak L, Niarchos D and Tzitzios V 2009 *J. Phys. Chem.* C **113** 14609
[14] Masala O and Seshadri R 2005 *J. Am. Chem. Soc.* **127** 9354
[15] Frandsen C, Ostenfeld C W, Xu M, Jacobsen C S, Keller L, Lefmann K and Mørup S 2004 *Phys. Rev.* B **70** 134416
[16] Ali M, Adie P, Marrows C H, Greig D, Hickey B J and Stamps R L 2007 *Nature Mater.* **6** 70
[17] Del Bianco L, Fiorani D, Testa A M, Bonetti E and Signorini L 2004 *Phys. Rev.* B **70** 052401
[18] Zheng R K, Wen G H, Fung K K and Zhang X X 2004 *Phys. Rev.* B **69** 214431
[19] Maletta H and Zinn W Jr 1989 *Handbook on the Physics and Chemistry of Rare Earths* vol 12, ed K A Gschneidner and L Eyring (Amsterdam: Elsevier) p 213
[20] de Almeida J R L and Thouless D J 1978 *J. Phys. A: Math. Gen.* **11** 983
[21] Joy P A, Anil Kumar P S and Date S K 1998 *J. Phys.: Condens. Matter* **10** 11049
[22] Kinzel W 1979 *Phys. Rev.* B **19** 4595
[23] El-Hilo M, O'Grady M K and Chantrell R W 1995 *J. Magn. Magn. Mater.* **140–144** 359
[24] Kodama R H, Berkowitz A E, McNiff E J and Foner S 1996 *Phys. Rev. Lett.* **77** 394
[25] Martínez B, Obradors X, Balcells L, Rouanet A and Monty C 1998 *Phys. Rev. Lett.* **80** 181
[26] Fernández-García M P, Gorria P, Blanco J A, Fuertes A B, Sevilla M, Boada R, Chaboy J, Schmool D and Grenèche J M 2010 *Phys. Rev.* B **81** 094418
[27] Binek C 2004 *Phys. Rev.* B **70** 014421